Stem Cell Reports
Article

ISSCR

OPEN ACCESS

IAP-Based Cell Sorting Results in Homogeneous Transplantable Dopaminergic Precursor Cells Derived from Human Pluripotent Stem Cells

Daniela Lehnen,[1,4] Serena Barral,[2,4,5] Tiago Cardoso,[3] Shane Grealish,[3] Andreas Heuer,[3] Andrej Smiyakin,[1] Agnete Kirkeby,[3] Jutta Kollet,[1] Harold Cremer,[2] Malin Parmar,[3] Andreas Bosio,[1] and Sebastian Knöbel[1,*]

[1]Miltenyi Biotec GmbH, 51429 Bergisch Gladbach, Germany
[2]Aix-Marseille University, CNRS, IBDM; Campus de Luminy, 13009 Marseille, France
[3]Developmental and Regenerative Neurobiology, Department of Experimental Medical Science, Wallenberg Neuroscience Center and Lund Stem Cell Center, Lund University, 22184 Lund, Sweden
[4]Co-first author
[5]Present address: UCL GOS Institute of Child Health, 30 Guilford Street, London WC1N 1EH, UK
*Correspondence: sebastian.knoebel@miltenyibiotec.de
http://dx.doi.org/10.1016/j.stemcr.2017.08.016

SUMMARY

Human pluripotent stem cell (hPSC)-derived mesencephalic dopaminergic (mesDA) neurons can relieve motor deficits in animal models of Parkinson's disease (PD). Clinical translation of differentiation protocols requires standardization of production procedures, and surface-marker-based cell sorting is considered instrumental for reproducible generation of defined cell products. Here, we demonstrate that integrin-associated protein (IAP) is a cell surface marker suitable for enrichment of hPSC-derived mesDA progenitor cells. Immunomagnetically sorted IAP$^+$ mesDA progenitors showed increased expression of ventral midbrain floor plate markers, lacked expression of pluripotency markers, and differentiated into mature dopaminergic (DA) neurons *in vitro*. Intrastriatal transplantation of IAP$^+$ cells sorted at day 16 of differentiation in a rat model of PD resulted in functional recovery. Grafts from sorted IAP$^+$ mesDA progenitors were more homogeneous in size and DA neuron density. Thus, we suggest IAP-based sorting for reproducible prospective enrichment of mesDA progenitor cells in clinical cell replacement strategies.

INTRODUCTION

Parkinson's disease (PD) is a common neurodegenerative disorder primarily involving degeneration of dopaminergic (DA) neurons in the substantia nigra (SN). DA neurons located in the SN project to the striatum where they release dopamine and have a crucial role in motor control. Preclinical studies, as well as clinical trials, have shown that transplantation of fetal mesencephalic tissue can restore dopaminergic activity and reduce motor symptoms in PD patients for up to 18 years (Barker et al., 2013, 2015; Kefalopoulou et al., 2014). Recent studies in animal models of PD suggest that DA progenitors differentiated from human pluripotent stem cells (hPSCs) constitute an alternative cell source for transplantation therapy, showing a similar capacity to fetal tissue in terms of ability for terminal differentiation capacity for integration and projection, regulated dopamine release, and functional recovery of Parkinsonian symptoms (Doi et al., 2014; Grealish et al., 2014; Kirkeby et al., 2012a; Kriks et al., 2011; Steinbeck et al., 2015). Therefore, transplantation of hPSC-derived mesDA neurons may constitute a promising future therapy for PD patients, suitable for the treatment of large cohorts.

While hPSC differentiation protocols have improved in terms of quality and reproducibility over the past years, it is a common observation that hPSC-derived differentiation cultures still represent heterogeneous mixtures of cells, containing a variety of phenotypes and degrees of maturity. Furthermore, resulting cell compositions vary between experiments and cell lines (Osafune et al., 2008). Also, the safety aspect is of paramount importance since remaining undifferentiated hPSCs pose a risk of teratoma formation after transplantation (Brederlau et al., 2006; Doi et al., 2012; Sonntag et al., 2007), and poorly differentiated cells with high proliferative capacity have been associated with neural tissue overgrowth *in vivo* (Lindvall and Kokaia, 2009). In addition, contaminating serotonergic neurons have been discussed as a possible contributing factor to graft-induced dyskinesia (Carlsson et al., 2007; Politis et al., 2010). Cell sorting is considered to be instrumental for reproducible generation of safe and defined functional cell products (Bye et al., 2015; Ganat et al., 2012; Tabar and Studer, 2014; Villaescusa and Arenas, 2010). Magnetic cell sorting has been reported to allow faster and gentler handling of cells (Bosio et al., 2009; Pruszak et al., 2007), stable engraftment, and survival of transplanted embryonic stem cell (ESC)-derived neural cells (Barral et al., 2013; Bryson et al., 2014). Importantly, magnetic cell sorting can be utilized in large-scale clinical procedures under sterile conditions (Despres et al., 2000; Schumm et al., 2013).

Previous rodent studies have identified CORIN, PSA-NCAM, and ALCAM (Bye et al., 2015; Friling et al., 2009; Ono et al., 2007) as mesDA progenitor-associated cell surface markers. Antibodies directed against CORIN, NCAM, and LRTM1 were also used to enrich hPSC-derived

dopaminergic neurons that could ameliorate motor symptoms in animal models of PD. However, in these studies, cells were either cultivated for an extended time between sorting (day 12) and transplantation (day 28/42) (Doi et al., 2014; Hargus et al., 2010; Samata et al., 2016) or were sorted and transplanted as late as day 42 (d42) of differentiation and in this case resulted in poor graft survival (Hargus et al., 2010).

No systematic marker identification studies have been reported for human mesDA cells. We screened a library of 312 annotated antibodies and discovered integrin-associated protein (IAP, CD47) as a cell surface marker suitable for immunomagnetic isolation of FOXA2$^+$ hPSC-derived mesDA progenitor cells with floor plate identity. IAP-based cell sorting may therefore contribute to the generation of more homogeneous cell products for future clinical use.

RESULTS

Identification of IAP as a Cell Surface Marker for mesDA Progenitor Cells

To identify a surface marker suitable for cell sorting, we performed a flow cytometry-based surface marker screen on hPSC-derived mesDA progenitor cells, generated based on the protocol developed by Kirkeby et al. (2012a) with minor modifications (Figure 1A).

We used two hPSC lines, one of embryonic origin (H9) and one hiPSC line originally derived from human foreskin fibroblasts (hFF-iPSC). Measurements were performed on d11 and d16 of differentiation to cover early as well as more mature mesDA progenitors. Since mesDA progenitors from both stages expressed FOXA2$^+$/LMX1A$^+$, we used FOXA2 counterstaining to identify the cells of interest and their correlation to a total of 312 surface markers. We identified 29 markers strongly expressed on the FOXA2$^+$ cells (>90% positive cells) in any of the cell lines or time points. Twelve of these surface markers were concomitantly expressed on d11 and d16 of differentiation in both H9 and hiPSC-derived FOXA2$^+$ cells (Figure 1B, Table S5). The surface marker IAP emerged as a suitable marker for cell sorting with superior discrimination between the FOXA2$^+$ target cells and FOXA2$^-$ non-target cells over all other markers tested (Figure 1C). The robust correlation of IAP and FOXA2 expression observed by flow cytometry analysis (Figures 1D and S1) could also be confirmed using immunofluorescence microscopy (Figure 1E) and using two more cell lines (hESC: SA001, hiPSC: hCBEC-iPSC; data not shown).

In order to characterize the IAP$^+$ cells more closely, further co-staining with known surface as well as intracellular markers were performed on hiPSC and hESC-derived mesDA progenitors on d11 and d16 and analyzed by flow cytometry (Figures 2A, 2B, and S2) Expression of the pluripotency marker OCT4 was negligible in both cell lines at d11 and d16. Likewise, SOX1 a primitive neuroectodermal marker later restricted to the lateral floor plate (Wood and Episkopou, 1999) was not expressed at these time points. SOX2 expression was slightly elevated in IAP$^+$ cells and decreased from d11 to d16. Expression of Ki67 diminished from nearly 100% in the pluripotent state (not shown) to 60%–40% at d11 and 50%–10% at d16, with the hESCs showing a faster drop in proliferation marker expression over time, as observed for SOX2. Absence of NKX2.1 confined to the forebrain and PAX6 expressed in the roof plate (Kirkeby et al., 2017) of the neural tube indicated that cells were patterned to a ventralized fate rostral of the midbrain hindbrain boundary. NCAM was broadly expressed on IAP$^-$ and IAP$^+$ cells at d11. At d16, 85% of the hiPSC-derived and 98% of the hESC-derived IAP$^+$ cells expressed NCAM. However, the IAP$^-$ fractions contained 17% and 66% NCAM$^+$ cells, respectively, indicating that IAP$^+$ cells represent a subpopulation of NCAM$^+$ cells. A comparable expression pattern was observed for PSA-NCAM. In contrast, CORIN expression was restricted to the IAP$^+$ cells already at d11. At d16, CORIN correlated nearly completely in the hESC-derived cells while only a subpopulation of the hiPSC-derived IAP$^+$ cells showed co-expression with CORIN, indicating that the CORIN fraction represents a subpopulation of the IAP$^+$ fraction. Since IAP is widely expressed in mesoderm-derived tissues, we analyzed the co-expression of IAP and prototypic mesodermal markers under the described differentiation conditions. The tested markers representing blood, endothelial, mesenchymal stromal, and epithelial cells were either not detected or negatively correlated (Figure S2).

Next, we analyzed the *in vivo* expression pattern of IAP in the developing neural tube of the human embryo. The neural tube can be subdivided in four domains along the ventro-dorsal axis: floor plate, basal plate, alar plate, and roof plate (Shimamura et al., 1995; Verney et al., 2001). Immunofluorescence analyses were performed on coronal sections of the ventral midbrain (VM) area of human embryos 7 weeks post conception (p.c.) (Figure 2B). As seen for their counterparts generated *in vitro*, IAP was indeed expressed in the FOXA2$^+$/LMX1A$^+$ floor plate cells predominantly in the midline and the mantle zone (Figure 2C). In addition, we detected IAP expression in the roof plate where it co-localized with LMX1A but not FOXA2. To translate and better understand the spatial distribution of IAP expression in the context of neural differentiation of hPSC, we mimicked the neural tube domains by patterning differentiating cells along the ventro-dorsal axis (Kirkeby et al., 2012b). As predicted, IAP showed a distinct co-expression with FOXA2 in the ventralized floor plate cells. Under basal plate induction conditions, FOXA2$^+$ cells expressed IAP to a certain

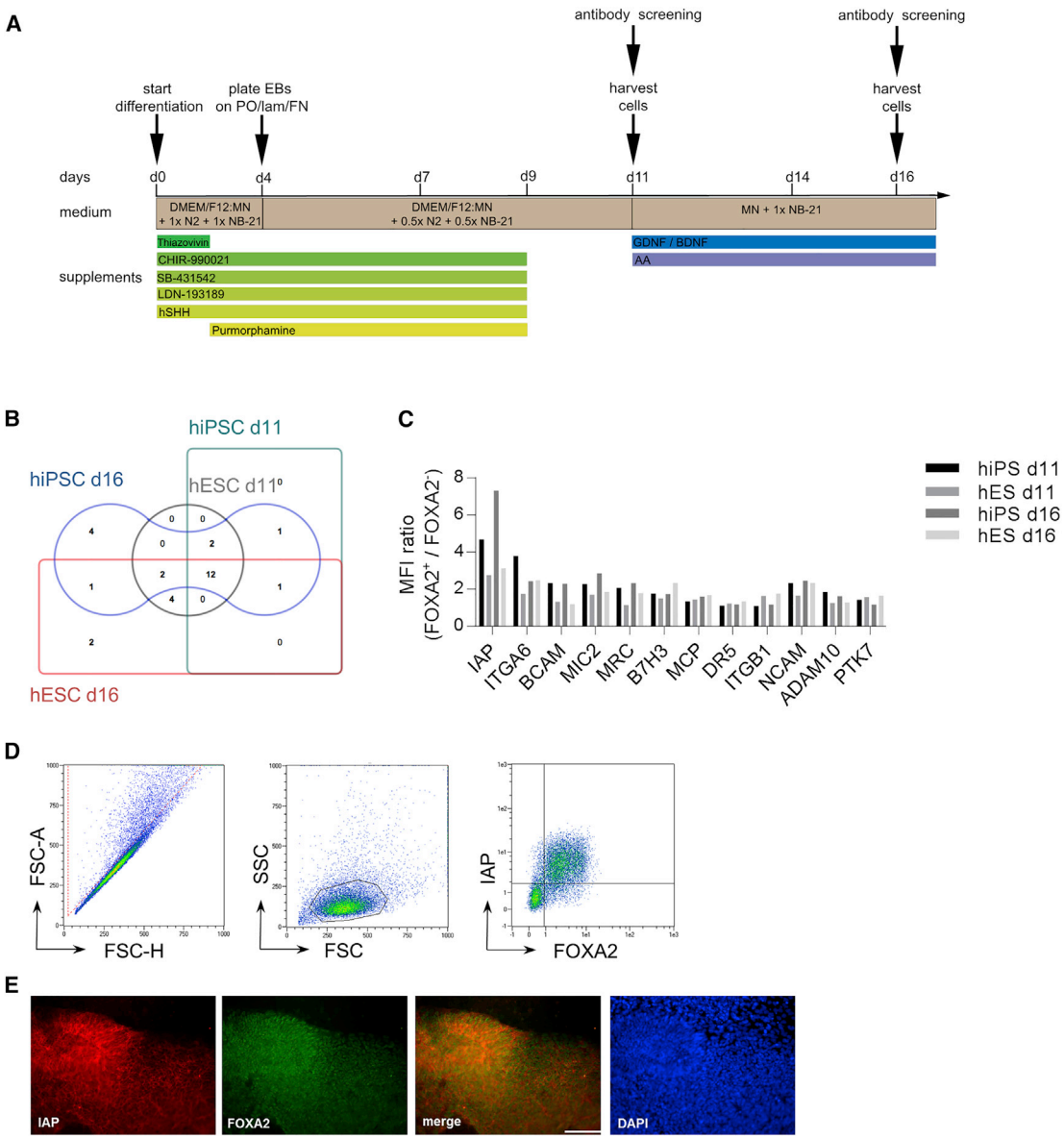

Figure 1. Identification of IAP as a Cell Surface Marker Expressed in FOXA2$^+$ mesDA Progenitor Cells

(A) mesDA were differentiated according to the protocol of Kirkeby et al. (2012a). Cells were harvested for a flow-cytometry-based surface marker screening on d11 and d16. AA, ascorbic acid; FN, fibronectin; lam, laminin; MN, MACS Neuro medium; NB-21, NeuroBrew-21; PO, poly-L-ornithine.

(B) hESCs (H9) and hiPSCs (hFF-iPS) were differentiated toward mesDA progenitor cells and screened for marker expression on d11 and d16 of differentiation. Surface markers expressed on >90% of the FOXA2$^+$ mesDA progenitor cells are depicted in the Edwards-Venn diagram (Bardou et al., 2014); see also Table S5. Twelve surface markers were concomitantly expressed on d11 and d16 in both hESC and hiPSC-derived FOXA2$^+$ cells.

(C) Comparative analysis of the 12 surface markers expressed in hESCs and hiPSCs at d11 and d16 of differentiation. Shown is the ratio of the mean fluorescence intensity (MFI) for each marker for FOXA2$^+$ and FOXA2$^-$ cells. IAP displayed the highest discrimination between FOXA2$^+$ and FOXA2$^-$ cells on hiPSCs and hESCs at d11 and d16.

(D) Schematic illustration of the gating strategy used for the cell surface marker screening. Single cells were distinguished by the FSC properties, and cells of interest were gated based on FSC/SSC characteristics. As shown for IAP, surface markers expressed by mesDA progenitors were identified based on the co-staining with FOXA2. See also Figure S1.

(E) Immunofluorescence staining of mesDA progenitor cells on d11 showed co-expression of IAP (red) and FOXA2 (green); Cell nuclei were stained with DAPI (blue). Scale bar represents 100 μm.

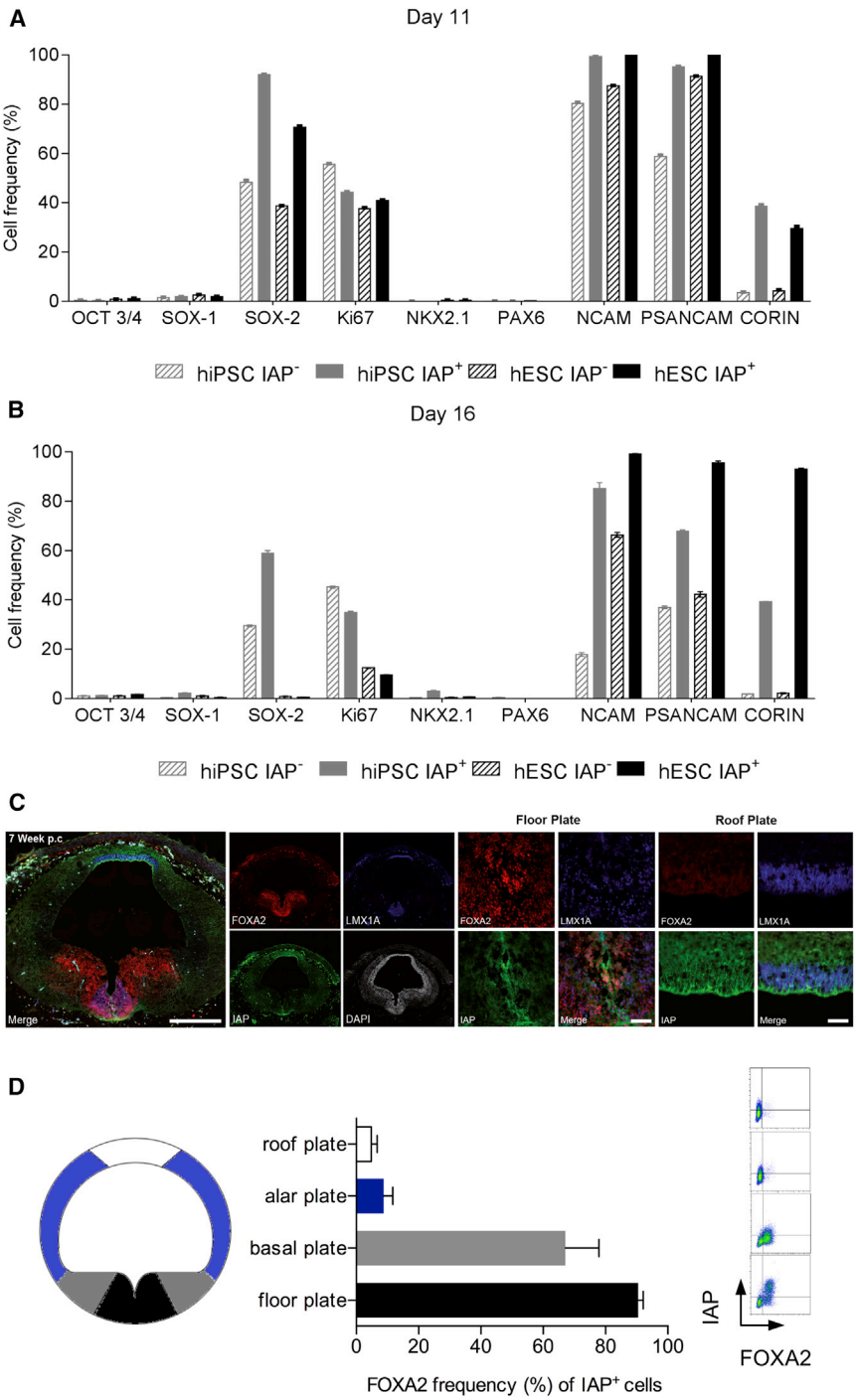

Figure 2. Characterization of IAP Expression *In Vitro* and *In Vivo*

(A and B) Flow cytometric analysis of IAP positive and negative cells on (A) d11 or (B) d16 of differentiation with respect to expression of known markers for pluripotent, neural (stem) cells. Bar graph shows the frequency of each marker expressed by the IAP^+ and IAP^- subsets for differentiated hESCs and hiPSCs as the mean of independent triplicates (mean ± SD). See also Figure S2.

(C) Protein expression in the neural tube of the human fetal mesencephalon (7 weeks p.c.). FOXA2 (red) is expressed within the floor plate and basal plate, LMX1A (blue) delineates the floor plate and the roof plate in human VM. IAP (green) expression was observed in the floor plate as well as in the roof plate. Cell nuclei stained with DAPI are shown in white. Scale bar represents 500 μm in the overview and 50 μm in close up.

(D) hiPSCs were differentiated toward floor plate, basal plate, alar plate, and roof plate fates, respectively. Color code indicates floor plate (black), basal plate (gray), alar plate (blue), and roof plate (white). Cells differentiated for 11 days *in vitro* were analyzed for IAP and FOXA2 expression using flow cytometry. Bar graphs illustrate the frequency (%) of $FOXA2^+$ cells in the IAP^+ fraction (n = 3; independent experiments; mean ± SD). Representative density plots are depicted for each differentiation condition.

frequency, but the expression level was much lower compared with floor plate patterned cells. In the alar and roof plate regimens, lower numbers of IAP-expressing cells and a lower expression level of IAP were detected (Figure 2D). In summary, IAP is suited for enrichment of hPSC-derived mesDA progenitors from ventrally patterned cells.

Immunomagnetic Sorting of IAP^+ Cells Allows for the Isolation of mesDA Progenitor Cells

Consequently, we established a sorting strategy for the enrichment of mesDA progenitor cells based on immunomagnetic isolation of IAP^+ cells (Figure 3A). Flow cytometric analyses of differentiated mesDA progenitor cells showed an initial frequency of IAP^+ cells of 49% ± 18.99% (n = 20) on

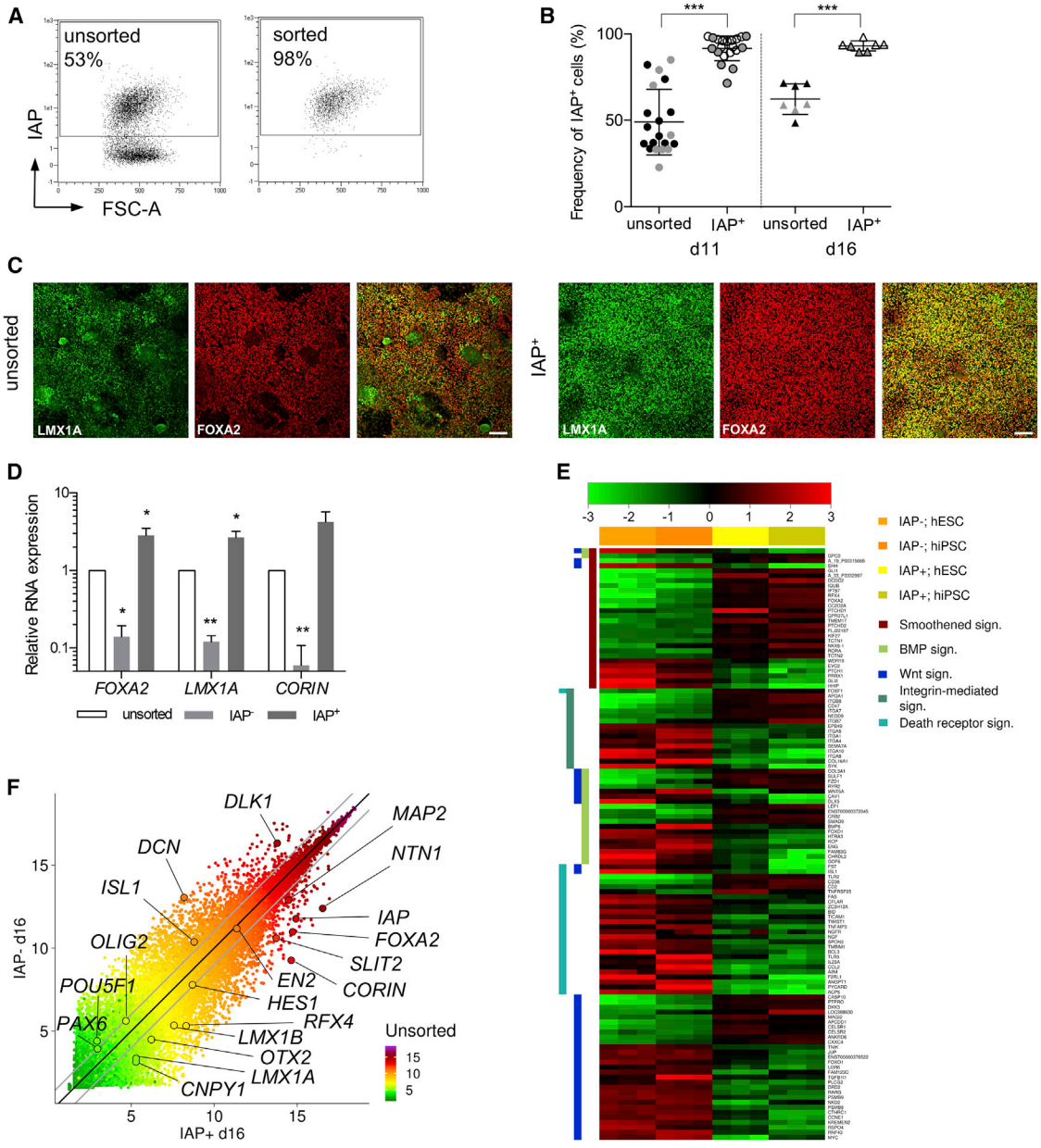

Figure 3. Purification and Characterization of IAP$^+$ mesDA Progenitor Cells

(A) The frequency of IAP$^+$ (d11) in the unsorted fraction accounted for 53% (left blot). After the immunomagnetic sorting, IAP$^+$ cells were enriched to a purity of 98%.

(B) Sorting efficiencies of IAP$^+$ cells derived from d11 and d16 of differentiation measured by flow cytometry. Gray symbols indicate differentiated hESCs and black symbols represent differentiated hiPSCs (d11 n = 20; d16 n = 7; independent experiments; mean ± SD; ***p < 0.005 according to Student's t test).

(C) Immunofluorescence analysis of the unsorted and IAP$^+$ cell fraction. LMX1A (green) and FOXA2 (red). LMX1A$^+$/FOXA2$^+$ cells are shown in the merged picture. In contrast to the unsorted cells, the IAP$^+$ cells reveal homogeneous FOXA2/LMX1A co-expression 3 days after replating. Scale bar represents 100 μm.

(D) Gene expression analysis for FOXA2, LMX1A, and CORIN on the unsorted, IAP$^-$, and IAP$^+$ cells by qRT-PCR. Values are shown as the relative expression of each gene compared with the unsorted fraction (n = 3; independent experiments; mean ± SD; *p < 0.05; **p < 0.005; according to Student's t test).

(E) IAP$^+$ versus IAP$^-$ cells sorted on d16 of differentiated hESCs and hiPSCs. The color represents log2 intensity values centered to the gene-wise median of all samples; saturation limits are indicated in the green-black-red color bar above the heatmap. The sample groups are

(legend continued on next page)

d11 and 62.30% ± 8.87% (n = 7) on d16, independent of the source of cells used, i.e., hiPSCs or hESCs. Immunomagnetic cell sorting enriched IAP$^+$ cells to 92.04% ± 6.87% (n = 20) on d11 and to 93.08% ± 2.94% (n = 7) on d16 of differentiation (Figure 3B). The viability of the IAP$^+$ cells was not affected by immunomagnetic sorting (99.37% ± 0.56%; n = 10) based on flow cytometric analyses. Therefore, IAP-based sorting results were highly consistent, independent of the starting frequency of IAP$^+$ cells or day of differentiation.

Sorted and unsorted cells were replated at d11 and further analyzed at d14 to elucidate FOXA2$^+$/LMX1A$^+$ co-expression using immunofluorescence. The IAP$^+$ cell population had a higher expression of FOXA2 and LMX1A compared with the unsorted cells (Figure 3C). qRT-PCR revealed that the expression levels of mesencephalic floor plate markers *LMX1A* and *FOXA2* were significantly higher in the IAP$^+$ cells compared with the unsorted fraction (Figure 3D), as well as the surface mesDA marker *CORIN*.

To further delineate the differences between the unsorted, IAP$^+$, and IAP$^-$ cells, we analyzed the gene expression profiles using a human whole-genome array. mesDA progenitor cells were sorted on d16 of differentiation (hiPSC and H9 hESC). The frequency of IAP$^+$ cells within the unsorted samples on d16 was 70.9% ± 0.9% (n = 3) for hiPSC and 58.2% ± 1.7% (n = 3) for hESC-derived mesDA progenitors. After sorting, only a small percentage of IAP$^+$ cells were retained in the negative fraction (5.9% ± 0.1% and 1.8% ± 1.2% respectively), while the corresponding IAP$^+$ cell fraction was enriched to 93.8% ± 0.1% and 90.7% ± 1.9%. Since the enrichment factor was 1.3 and 1.5 for hiPSCs and hESCs, respectively, we expected only minor differences between the unsorted and IAP$^+$ fraction using global expression analyses. Therefore, we focused on comparative analysis of the IAP$^+$ and IAP$^-$ fractions in order to characterize the IAP$^+$ cells further.

Pathway analysis of the significant differentially expressed genes between the d16 IAP$^+$ and IAP$^-$ fractions showed regulation of pathways involved in midbrain development, specifically Smoothened, BMP, and WNT pathways (Figures 3E and S3). Furthermore, regulation of genes associated with Integrin and death receptor pathway could be detected. The respective up- or downregulation of key genes of these pathways resembled the stronger response and adaptation of the IAP$^+$ cells to the patterning cues of the differentiation process.

Mesencephalic-specific genes and mesDA progenitor-associated genes such as *FOXA2*, *FOXA1*, *LMX1A*, *LMX1B*, *RFX4*, *SLIT2*, *CNPY1* (Kirkeby et al., 2017; La Manno et al., 2016), and *CORIN* were higher expressed in the IAP$^+$ cells compared with the IAP$^-$ cells (Figure 3F). Furthermore, non-neural genes, such as *DLK1*, genes associated with non-VM neural fates (e.g., *DECORIN*, *PAX6*, *SIX3*), and genes associated with pluripotency, such as *POU5F1* and *NANOG* were either expressed at a low level after 16 days of *in vitro* differentiation or, if detected, showed higher expression in the IAP$^-$ fraction (Figure 3F).

The potential of the sorted cells to develop into dopaminergic neurons was assessed by replating the unsorted, IAP$^+$, and IAP$^-$ fractions after sorting on d16 and subsequent terminal differentiation *in vitro* until d50. Immunofluorescence analyses for the neural marker TUJ1 and the dopamine neuron marker TH showed a high level of co-expression (Figure 4A). qRT-PCR analyses revealed that mesencephalic genes such as *LMX1A* and *LMX1B* were expressed to the same extent in the unsorted fraction as in the IAP$^+$ fraction, while higher expression of *FOXA2* was observed in the IAP$^+$ fraction, implying a mesDA phenotype. *EN1*, *TH*, and *SYP-1* were expressed in the IAP$^-$ fraction to a significantly higher extent compared with the unsorted fraction. Interestingly, we observed lower serotonergic gene expression, *TPH2* and *SERT*, in the IAP$^+$ fraction compared with the IAP$^-$ fraction (Figures 4B and S4).

Further pathway analyses of the differentially expressed genes between the IAP$^+$ cells at d16 of differentiation and d16 sorted and terminally differentiated IAP$^+$ cells until d50 clearly showed associations of the upregulated genes with dopamine, neuropeptide, and glutamate signaling pathways in the terminally differentiated fraction (Figure 4C). As expected, genes for mature neurons were upregulated in the terminally differentiated cells (*BDNF*, *TH*, *KCNJ6*). Also genes associated with neurite outgrowth such as Osteoglycin (*OGN*) and dopamine receptor genes (*DRD2*, *DRD4*) were detected in the d50 cell fraction. In contrast, expression of genes associated with early mesDA progenitors was higher in the cells sorted and harvested on d16 (*FOXA2*, *OTX1*, *HES5*) (Figure 4D).

The phenotype of DA neurons derived from IAP$^+$ cells was additionally assessed by comparing expression trends between IAP$^+$ cells at d16 and d50 cells derived thereof with the expression difference of human embryonic neural stem cells (NSCs) and *in vivo* tissue samples from mature human DA neurons (Marei et al., 2011). For this, the expression values of IAP$^+$ d16 samples were plotted against

depicted by orange/yellow color bars above the heatmap. Shown is a selection of significantly enriched pathways associated with the candidate genes (see color bars on the right-hand side of the heatmap). See also Figure S3.

(F) Gene expression trends of hESC-derived mesDA progenitors d16 unsorted, IAP$^+$, and IAP$^-$ samples are summarized in scatterplots. The unfiltered normalized log2 intensities of IAP$^-$ versus IAP$^+$ cells are compared. The color code corresponds to the median values of the normalized log2 intensities of independent experiments of the unsorted fraction.

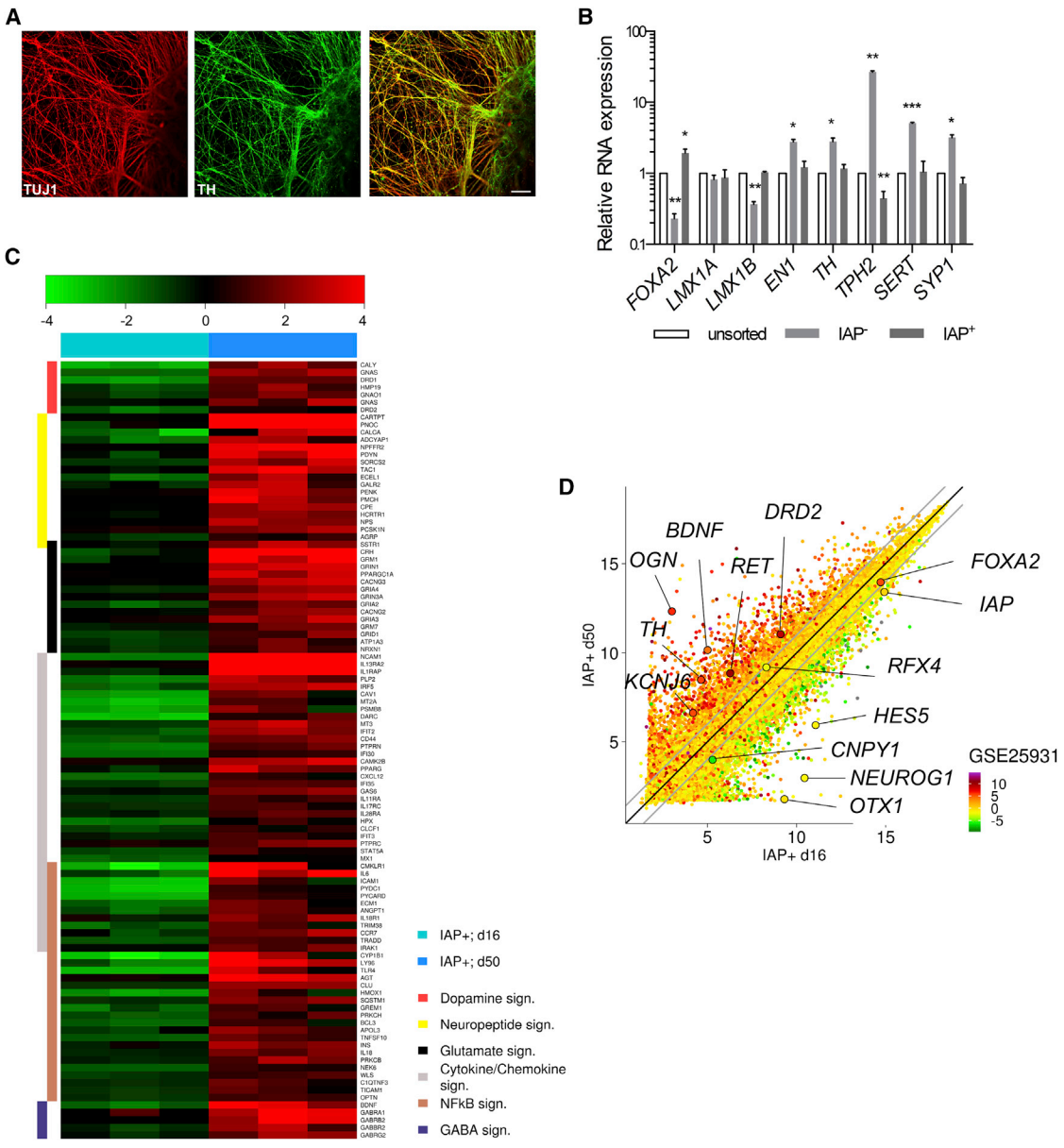

Figure 4. Gene Expression and Pathway Analysis of d16 Sorted IAP$^{-/+}$ Fractions and d16 IAP^{+} Cells Terminally Differentiated until d50

(A) Immunofluorescence staining of differentiated hESCs, positively sorted for IAP on d16 and replated for terminal differentiation until d50. Mature dopaminergic neurons are detected by TH (green) and TUJ1 (red) co-staining (shown as merged picture). Cell nuclei were stained with DAPI (blue). Scale bar represents 100 μm.

(B) Gene expression analysis (qRT-PCR) of differentiated hESCs at d50. Sorting was performed at d16 of differentiation of hESCs, and unsorted, IAP^{-}, IAP^{+} cell fractions were replated for terminal differentiation. Shown is the mRNA expression of selected genes within the IAP^{+} and the IAP^{-} fractions relative to the expression of the unsorted fraction (n = 3; independent experiments; mean ± SD; *p < 0.05; **p < 0.005; ***p < 0.0005). See also Figure S4.

(C) IAP^{+} cells sorted on d16 versus IAP^{+} cells sorted on d16 and subsequently differentiated until d50. The color represents log2 intensity values centered to the gene-wise median of all samples; saturation limits are indicated in the green-black-red color bar above the heatmap. The sample groups are depicted by blue color bars above the heatmaps. Shown is a selection of significantly enriched pathways associated with the candidate genes (see color bars on the right-hand side of the heatmaps).

(D) The d16 sorted IAP^{+} sample set versus IAP^{+} cells sorted on d16 and subsequently differentiated until d50. The color code corresponds to the log2-fold change values of adult human dopaminergic neurons relative to human embryonic NSCs (GEO: GSE25931) (Marei et al., 2011).

those of the d50 samples, and color coded by the fold-change difference between mature human DA neurons and human embryonic NSCs (Figure 4D). The majority of genes with higher expression after 50 days of culture compared with IAP$^+$ cells isolated on d16 also showed higher expression *in vivo* in DA neurons of adult human brains than in human embryonic NSCs.

From these data, we concluded that sorting of IAP$^+$ cells led to a cell population highly enriched for mesDA progenitors and, at the same time, purged of cells with undesirable phenotypes, such as serotonergic progenitors. Furthermore, the *in vitro* differentiation study of sorted mesDA progenitor cells confirmed their capability to differentiate into mature cells with phenotypic characteristics of dopaminergic neurons.

IAP$^+$-Enriched Dopaminergic Progenitor Cells Survive *In Vivo* and Differentiate to Mature Dopaminergic Neurons

To assess the *in vivo* performance of IAP-sorted cells, unsorted cells and IAP$^+$ cells from differentiated hiPSCs were grafted intrastriatally into 6-OHDA-lesioned adult rats kept under cyclosporin-mediated immunosuppression for the duration of the experiment. We compared different time points of sorting and transplantation to determine the best regimen for transplantation in a 6-week survival experiment (Figure 5A). One approach was to harvest mesDA progenitor cells on d11 and transplant the immunomagnetically sorted and unsorted cells. In a second set, cells immunomagnetically sorted on d11 were replated for transplantation on d16. Lastly, cells were immunomagnetically sorted on d16, and sorted as well as unsorted cells were transplanted immediately. All grafts were analyzed 6 weeks after transplantation. For the cells transplanted on d11, we could not detect surviving cells regardless of whether they were sorted or unsorted. All other conditions transplanted on d16 resulted in neuron-rich grafts as determined by staining for human-specific NCAM (hNCAM) (Figures 5B–5D). Grafts of the sorted cells were smaller and had a more uniform graft size (Figure 5I). All animals with surviving grafts contained TH$^+$ neuron-rich grafts (Figures 5E–5G). Notably, while the TH count per graft was lower for the sorted conditions, the TH density was higher. Cells sorted and transplanted at d16 showed the highest TH cell density and displayed the most mature morphology (Figures 5H–5J).

In order to assess the full potential of the IAP$^+$ population, we performed long-term experiments to address if the resulting grafts were functional in a rat model of PD. For this purpose, hESCs (H9) were differentiated to a VM fate, thereby focusing on the preferential transplantation regimen identified in the survival study, i.e., the IAP$^+$ population was sorted and grafted after 16 days (Figure 6A). Eighteen weeks post transplantation hNCAM-rich grafts were observed in both the unsorted (Figure 6B) and IAP-sorted groups (Figure 6D). Both groups generated grafts dense with TH$^+$ neurons (Figures 6C and 6E). Grafts from sorted cells displayed a higher density of TH$^+$ neurons (Figure 6F) than those from unsorted cells, while the general cell density was comparable (Figure S5A). TH neurons were clearly biased toward a GIRK2$^+$ over a CALB$^+$ phenotype (Figures 6G and S5B), the ratio being comparable in both groups. However, grafts from IAP$^+$ cells contained significantly less serotonergic neurons (Figure 6H) and slightly fewer proliferative cells than grafts from unsorted cells (Figure S5C).

The functionality of the TH$^+$ neurons was assessed using amphetamine-induced rotation. Both groups demonstrated complete functionality without lateral rotational bias after 18 weeks (Figure 6I, n = 3 per group). Importantly, the grafts from the sorted cells were smaller than their counterparts from unsorted cells, and contained a modest total number of TH$^+$ neurons (5,200, 3,900, 840). This showed that IAP-sorted cells can function near equipotency of human fetal cells (Rath et al., 2013), as was also previously demonstrated using unsorted hESC-derived DA neurons (Grealish et al., 2014; Kirkeby et al., 2012a).

In summary, this dataset demonstrates that d16-sorted IAP$^+$ mesDA progenitors survive and mature long term and provide functional recovery in a rodent model of PD.

DISCUSSION

Our unbiased screening of 312 annotated antibodies led to the identification of 12 candidate markers expressed predominantly on FOXA2$^+$ cells at d11 and d16 of differentiation, both for hESC and hiPSC-derived mesDA progenitor cells. An antibody against IAP (CD47) allowed the most reliable discrimination of FOXA2$^+$ and FOXA2$^-$ cells and thereby enabled prospective isolation of mesDA progenitor cells. IAP is a five-span membrane protein and a member of the immunoglobulin superfamily. Most likely it has tissue-specific isoforms and associates with integrins (Reinhold et al., 1995). In mice, IAP is widely expressed in the brain, especially in synapse-rich regions, and several functions have been attributed to IAP in the developing mouse brain (Huang et al., 1998; Jiang et al., 1999; Mi et al., 2000; Ohnishi et al., 2005). However, little is known about the expression specificity of IAP in the developing human brain. In particular, the specific role of IAP in hPSC-derived dopaminergic progenitor cells remains to be elucidated.

Screening against FOXA2 allowed us to initially identify markers associated with ventralized fates. Parallel screening for LMX1A positivity was simply impeded by the lack of antibodies suitable for flow cytometry. Therefore, regional

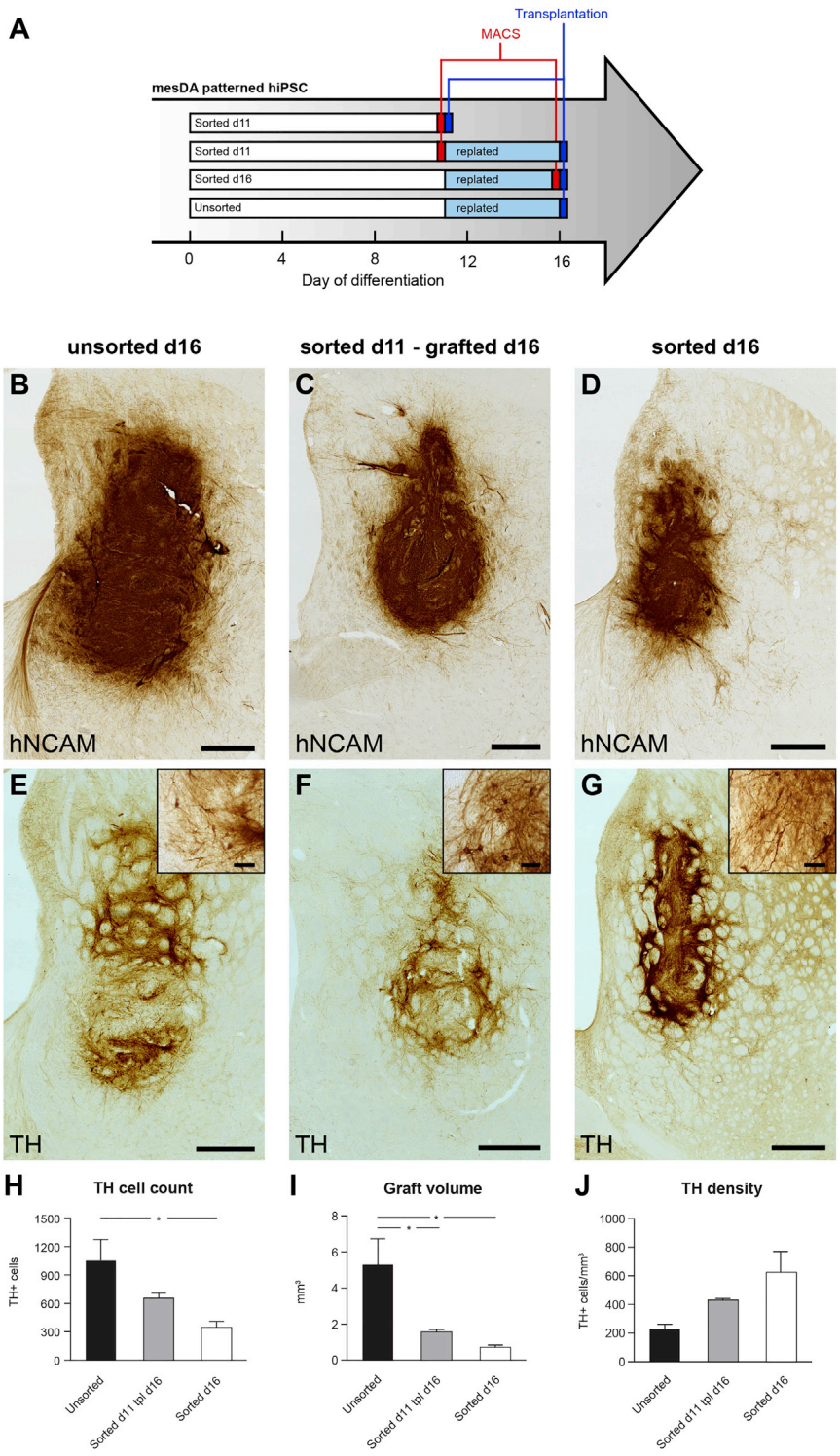

Figure 5. Six Week Survival of Unsorted versus IAP$^+$ hiPSC-Derived mesDA Progenitors Grafted to the Striatum

Schematic experimental setup (A) and histological analysis of grafts (B–G) 6 weeks after intrastriatal transplantation. Cells were either transplanted on d11 (no grafts detected) or d16 immediately after IAP-based immunomagnetic enrichment (D and G) or sorted on d11, replated and transplanted at d16 (C and F), or transplanted on d16 without sorting (B and E). Immunohistochemistry for hNCAM (B–D) and TH (E–G) revealed that sorted cells gave rise to smaller grafts (I) with overall lower TH cell (H) count but higher TH density (J). Transplanted animals: unsorted, n = 4; sorted d11 tpl d16, n = 4; sorted d16, n = 5; mean ± SD; *p < 0.05 according to one-way ANOVA followed by Bonferroni post hoc test; using IBM SPPS Statistics. Scale bar represents 500 μm in (B–G) and 50 μm in close-up box (E–G). tpl, transplantation.

identity, i.e., co-expression of FOXA2 and LMX1A, had to be ensured by independent microscopic immunofluorescent analysis. We could validate that, under given differentiation conditions, the surrogate marker FOXA2 would at the same time be indicative of mesDA progenitors with correct rostro-caudal patterning (Kirkeby et al., 2012a; Kriks et al., 2011). Analyzing sections of the human fetal mesencephalon (7 weeks p.c.) revealed that some IAP expression

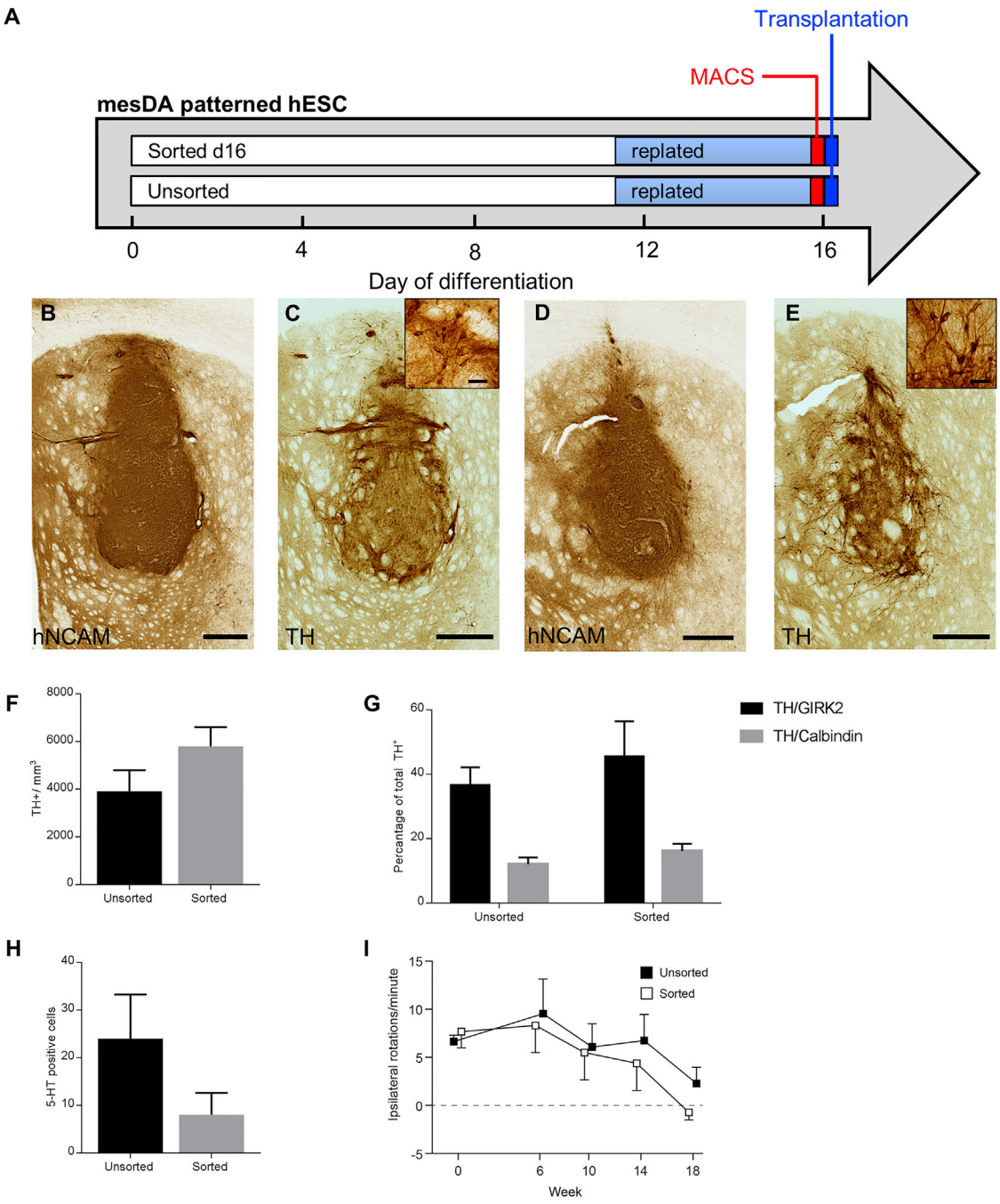

Figure 6. Functional Potency Assessment of Unsorted versus IAP$^+$ hESC-Derived mesDA Progenitors Grafted to the Striatum

Schematic experimental setup (A) and histological analysis of grafts (hNCAM: B, D; TH: C, E) 18 weeks after intrastriatal transplantation. Transplantation of immunomagnetically enriched d16 IAP$^+$ mesDA progenitors yielded grafts with higher TH density than from unsorted control cells (F), see also Figure S5. Proportion of TH$^+$ neurons coexpressing GIRK2 and Calbindin was comparable (G) the number of 5-HT$^+$ cells was lower in grafts form IAP$^+$ cells (H). IAP$^+$ progenitors like the controls led to complete functional recovery in an amphetamine-induced rotation assay 18 weeks after grafting (I). Transplanted animals: unsorted, n = 3; sorted, n = 3; mean ± SD. Scale bar represents 500 μm in (B–E) and 50 μm in close-up box (C and E).

was detectable in the roof plate and the midline of the floor plate region. Consequently, a weak expression of IAP could also be detected *in vitro* when cells were deliberately dorsalized. Upon ventralizing differentiation conditions, IAP reliably identified FOXA2$^+$/LMX1A$^+$ mesDA progenitors. This observation underlines the importance of using high-quality raw material and standardized protocols to ensure proper patterning but also independent quality control procedures for phenotyping of the resulting cell product.

Comparative flow cytometry characterization of the IAP$^+$ and IAP$^-$ fraction on the protein level at d11 and d16 as well as gene expression analysis on d16 of differentiation revealed that IAP-based sorting led to enrichment of a cell population with correctly specified floor plate cells, as indicated by a higher expression of specific markers such as *LMX1A*, *LMX1B*, and *FOXA2*. IAP$^+$ cells had established a *FOXA2* expression circuitry as indicated by upregulation of the *FOXA2* target genes *SHH*, *FOXA1*, *FERD3L (NATO3)*, and *SLIT2* and repression of SHH signaling pathway components such as *PATCHED-1* and *-2*, *GLI-1* and *-2* (Metzakopian et al., 2012), remarkably, 7 days after ventralizing factors SHH and purmorphamine had been removed from the cultivation media. However, this transient cell state seems to be dependent on further signaling to exert the full DA neuron differentiation potential, as under the subsequent neuronal differentiation conditions d16 IAP$^+$ cells did not yield more TH neurons than unsorted cells or even IAP$^-$ cells *in vitro*. Reasons for the latter observation could be the asynchrony of differentiation cultures, as well as the limited ability to mimic the rigorous developmental fate instruction *in vitro*. Similarly, Aguila et al. (2014) failed to enrich dopaminergic neurons in subsequent differentiation after sorting neuronal progenitors based on FOXA2-promoter driven GFP-expression. Nonetheless, our cells sorted for IAP at d16 and *in vitro* differentiated to d50 expressed genes related to mature dopaminergic neurons (*TH*, *DRD2*, *DAT*). Furthermore, these cells displayed lower relative gene expression of serotonergic specific genes (*TPH-2*, *SERT*) *in vitro*, which suggests a qualitative advantage connected to the IAP-based progenitor selection. However, further studies need to address this in more detail since the temporal aspects as well as downstream differentiation conditions could have a major impact on the final differentiation outcome. Notably, in mouse floor plate cells, SHH expression was shown to inhibit neuronal differentiation, and WNT/β-catenin signaling is necessary and sufficient for antagonizing SHH, DA progenitor marker induction, and promotion of dopaminergic neurogenesis (Joksimovic et al., 2009). These findings might add to further refinement of DA neuron terminal differentiation *in vitro*.

More importantly, our *in vivo* study revealed the value of IAP-based selection. We were able to demonstrate that intrastriatal transplantation of sorted hESC-derived IAP$^+$ cells could revert the motor symptoms in 6-OHDA-lesioned rats and resulted in mature grafts after 18 weeks without compromising cell survival, maturation, innervation, or function. Beyond that, grafts from IAP$^+$ cells contained less 5-HT$^+$ serotonergic neurons than grafts from unsorted cells, which by itself is a very desirable feature since serotonergic neurons are deemed to cause graft-induced dyskinesia. In contrast to previous studies, target cells could be selected after only 16 days of differentiation and immediately transplanted without the need for prolonged *in vitro* manipulation as reported for other protocols (Doi et al., 2012; Hargus et al., 2010; Samata et al., 2016). IAP$^+$ cells gave rise to functional grafts without signs of overgrowth or teratoma formation, thereby addressing the concern related to hPSC-derived cell products. Grafts from sorted cells had a higher TH density (i.e., TH$^+$ cells/mm^3) but were smaller and contained fewer TH cells and less proliferative cells than the control grafts. This might be caused by cells with a higher proliferative potential in the IAP$^-$ fraction within these grafts. This compares well with the observations *in vitro* indicating that some cells with epithelial character (CD324 and CD326 positive cells) could be observed in IAP-negative fractions at d16 of differentiation. Vice versa this would imply that IAP$^+$ cells tend to mature faster into postmitotic cells *in vivo*. Finally, the increased homogeneity of transplant size and function observed in grafts obtained from the sorted cell fraction should increase the predictability of graft size and thus facilitate dosing.

Notably, the occurrence of teratomas or neural overgrowths has not been a matter of concern for well-differentiating hESCs such as H9 when applying new-generation floor plate induction protocols (Grealish et al., 2014; Kirkeby et al., 2012a; Kriks et al., 2011). However, other cell lines may exhibit less favorable risk profiles. Although differentiation efficiencies have been constantly optimized (Kirkeby et al., 2017), cell-line-specific variations cannot be excluded. Therefore, cell sorting could increase the safety and functionality of grafts from a broader range of cell sources.

From a translational perspective, our study clearly emphasizes the utility for IAP-based cell sorting of heterogeneous cell populations in order to meet safety and quality requirements for future therapeutic cell products.

EXPERIMENTAL PROCEDURES

Human Fetal Tissue

Human fetal tissue was obtained from legally terminated embryos with approval of the Swedish National Board of Health and Welfare in accordance with existing guidelines, including informed consent from women seeking elective abortions. The gestational age of each embryo was determined by measuring the crown-to-rump length and/or estimated by ultrasound measurements. Embryos were then staged according to weeks post conception.

Human iPSC and ESC Culture

hFF-iPSCs were maintained on gamma-irradiated CF1-MEFs in DMEM/F12 (Gibco) supplemented with 20% KnockOut-Serum Replacement (Gibco), 0.1 mM 2-mercaptoethanol, 1% Pen/Strep (Lonza), 1% non-essential amino acid solution, 2 mM L-glutamine, 8 ng/mL human FGF-2 (Miltenyi Biotec) or on Matrigel (BD Bioscience) in StemMACS iPS-Brew XF (Miltenyi Biotec). hESCs (SA001 and H9) were cultivated on feeders as described above but in KO-DMEM and DMEM/F12 (Gibco), respectively.

Cells were passaged with TrypLE or EDTA (Thermo Fisher Scientific) every 4–7 days. Cells were replated at a density of 8,000–12,500 cells/cm^2 in medium supplemented with ROCK inhibitor (Thiazovivin 2 μM; Miltenyi Biotec) for the first 48 hr. Afterward, media change was conducted daily.

Differentiation of hiPSCs and hESCs

The mesDA-differentiation protocol was adapted from Kirkeby et al. (2012b) with minor modifications as specified in Supplemental Experimental Procedures.

Dorsoventral patterning of neural progenitors (11 days) was performed as described in Kirkeby et al. (2012b).

Immunomagnetic Cell Separation of Differentiated Cells on d11 or d16

Differentiated cells were harvested with Accumax and separation was performed using an indirect immunomagnetic labeling strategy. In brief, for positive enrichment, 5 × 10^6 single cells were stained in 0.1 mL PEB buffer (PBS/2 mM EDTA/0.5% BSA) with primary antibody (CD47-PE [Clone REA220], Miltenyi Biotec; titer 1:30) for 10 min at 4°C. Cells were washed with 2 mL of medium, centrifuged, and then incubated for 15 min at 4°C in 0.1 mL of a 1:5 dilution of anti-PE-MicroBeads (Miltenyi Biotec) in medium. Cells were washed with medium, centrifuged, and resuspended in 0.5 mL of medium. To obtain the negative fraction, depletion of IAP was performed using the same procedure but increasing the titer of primary antibody to 1:10. In order to achieve higher purity for enrichment of IAP$^+$ cells, a second MS column was used. After separation, cells were either investigated by flow cytometry or seeded for further differentiation and immunofluorescence analysis.

The antibody derived from the clone REA220 specifically blocks binding of the widely used monoclonal antibody B6H12, indicating that REA220 recognizes the same surface epitope as the monoclonal antibody B6H12 (Figure S1).

Flow Cytometry

In order to distinguish different cell lines in one screening approach, a CellTrace Violet Cell Proliferation Kit (Violet Dye, Life Technologies) was used with a concentration of 2 μM according to the manufacturer's protocol.

For surface marker staining, primary antibody staining was performed in PEB buffer for 10 min at 4°C. After washing in PEB, secondary staining was performed for 10 min at 4°C. APC-conjugated antibodies were used for the screening experiments (MACS Marker Screen, human; prototype with reduced set of surface markers; Miltenyi Biotec). Intracellular epitopes were stained using the FoxP3 Buffer Set (Miltenyi Biotec) after surface marker staining. In brief, cells were fixed for 30 min at 4°C. After the washing step, the intracellular antibody was diluted in 1× Perm buffer and incubated for 30 min at 4°C, washed, and resuspended in a suitable volume of PEB buffer. Single cells were discriminated by FSC-A and FSC-H properties. In the next gate, forward scatter (FSC) was applied against the side scatter (SSC) to mark the population of interest. Propidium iodide was used for discrimination of dead cells only if cells were not permeabilized before. The gates for the fluorescence channel were set according to unstained and isotype controls. Data were acquired using the MACSQuant Analyzer 10 and analyzed with the MACSQuantify Software (Miltenyi Biotec). Antibodies used for flow cytometry and immunocytochemistry are listed in Tables S1 and S2, respectively.

Microarray Analyses and qRT-PCR

Microarray and RT-PCR analysis were conducted following standard procedures. The microarray data are available at NCBI GEO with accession number GEO: GSE74991. For further details see Supplemental Experimental Procedures. Differentially expressed genes (microarray analyses) are listed in Table S3. Primers are listed in Table S4.

Experimental Animal Studies

Adult female Sprague-Dawley rats (225–250 g; Charles River) were housed in a 12-hr light/dark cycle with *ad libitum* access to food and water. All experimental procedures were conducted following the guidelines of the Ethical Committee for the use of Laboratory Animals in Lund University. All procedures were conducted in accordance with the European Union Directive (2010/63/EU) and were approved by the Ethical Committee for the use of laboratory animals at Lund University and the Swedish Department of Agriculture (Jordbruksverket). For further details, see Supplemental Experimental Procedures.

Statistical Analysis

Statistical analysis was performed with GraphPad Prism6 unless stated otherwise. All pooled data are presented as means ± SD. Statistical tests and the number of independent experiments relevant for individual experiments are stated in the figures legends.

ACCESSION NUMBERS

The accession number for the gene expression datasets reported in this paper is GEO: GSE74991.

SUPPLEMENTAL INFORMATION

Supplemental Information includes Supplemental Experimental Procedures, five figures, and five tables and can be found with this article online at http://dx.doi.org/10.1016/j.stemcr.2017.08.016.

AUTHOR CONTRIBUTIONS

Conceptualization, S.K. and A.B.; Methodology, D.L. and S.B.; Investigation, D.L., A.S., S.B., A.H., T.C., S.G., and A.K.; Data Curation, J.K. and D.L.; Writing – Original Draft, D.L. and S.K; Writing – Review & Editing, D.L., S.K., A.B., and M.P.; Funding Acquisition, H.C., A.B., and M.P.; Supervision, S.K., A.B., H.C., and M.P.

ACKNOWLEDGMENTS

We would like to acknowledge Silvia Rüberg, Michail Knauel, Timon Hick, and Annett Kurtz for data processing and technical assistance. This study was supported by grants from the European Community's 7th Framework Program through DopaNew (286021), NeuroStemcellRepair (602278), ERC Grant Agreement (309712), and the Swedish Research Council. S.G. was supported by a postdoctoral stipend from the Swedish Brain Foundation (Hjärnfonden). M.P. is a New York Stem Cell Foundation Robertson Investigator. D.L., A.S., J.K., A.B., and S.K. are employees of Miltenyi Biotec.

Received: December 13, 2015
Revised: August 23, 2017
Accepted: August 24, 2017
Published: September 21, 2017

REFERENCES

Aguila, J.C., Blak, A., van Arensbergen, J., Sousa, A., Vazquez, N., Aduriz, A., Gayosso, M., Lopez Mato, M.P., Lopez de Maturana, R., Hedlund, E., et al. (2014). Selection based on FOXA2 expression is not sufficient to enrich for dopamine neurons from human pluripotent stem cells. Stem Cells Transl. Med. *3*, 1032–1042.

Bardou, P., Mariette, J., Escudie, F., Djemiel, C., and Klopp, C. (2014). jvenn: an interactive Venn diagram viewer. BMC Bioinformatics *15*, 293.

Barker, R.A., Barrett, J., Mason, S.L., and Bjorklund, A. (2013). Fetal dopaminergic transplantation trials and the future of neural grafting in Parkinson's disease. Lancet Neurol. *12*, 84–91.

Barker, R.A., Drouin-Ouellet, J., and Parmar, M. (2015). Cell-based therapies for Parkinson disease-past insights and future potential. Nat. Rev. Neurol. *11*, 492–503.

Barral, S., Ecklebe, J., Tomiuk, S., Tiveron, M.C., Desoeuvre, A., Eckardt, D., Cremer, H., and Bosio, A. (2013). Efficient neuronal in vitro and in vivo differentiation after immunomagnetic purification of mESC derived neuronal precursors. Stem Cell Res. *10*, 133–146.

Bosio, A., Huppert, V., Donath, S., Hennemann, P., Malchow, M., and Heinlein, U.A. (2009). Isolation and enrichment of stem cells. Adv. Biochem. Eng. Biotechnol. *114*, 23–72.

Brederlau, A., Correia, A.S., Anisimov, S.V., Elmi, M., Paul, G., Roybon, L., Morizane, A., Bergquist, F., Riebe, I., Nannmark, U., et al. (2006). Transplantation of human embryonic stem cell-derived cells to a rat model of Parkinson's disease: effect of in vitro differentiation on graft survival and teratoma formation. Stem Cells *24*, 1433–1440.

Bryson, J.B., Machado, C.B., Crossley, M., Stevenson, D., Bros-Facer, V., Burrone, J., Greensmith, L., and Lieberam, I. (2014). Optical control of muscle function by transplantation of stem cell-derived motor neurons in mice. Science *344*, 94–97.

Bye, C.R., Jonsson, M.E., Bjorklund, A., Parish, C.L., and Thompson, L.H. (2015). Transcriptome analysis reveals transmembrane targets on transplantable midbrain dopamine progenitors. Proc. Natl. Acad. Sci. USA *112*, E1946–E1955.

Carlsson, T., Carta, M., Winkler, C., Bjorklund, A., and Kirik, D. (2007). Serotonin neuron transplants exacerbate L-DOPA-induced dyskinesias in a rat model of Parkinson's disease. J. Neurosci. *27*, 8011–8022.

Despres, D., Flohr, T., Uppenkamp, M., Baldus, M., Hoffmann, M., Huber, C., and Derigs, H.G. (2000). CD34+ cell enrichment for autologous peripheral blood stem cell transplantation by use of the CliniMACs device. J. Hematother. Stem Cell Res. *9*, 557–564.

Doi, D., Morizane, A., Kikuchi, T., Onoe, H., Hayashi, T., Kawasaki, T., Motono, M., Sasai, Y., Saiki, H., Gomi, M., et al. (2012). Prolonged maturation culture favors a reduction in the tumorigenicity and the dopaminergic function of human ESC-derived neural cells in a primate model of Parkinson's disease. Stem Cells *30*, 935–945.

Doi, D., Samata, B., Katsukawa, M., Kikuchi, T., Morizane, A., Ono, Y., Sekiguchi, K., Nakagawa, M., Parmar, M., and Takahashi, J. (2014). Isolation of human induced pluripotent stem cell-derived dopaminergic progenitors by cell sorting for successful transplantation. Stem Cell Reports *2*, 337–350.

Friling, S., Andersson, E., Thompson, L.H., Jonsson, M.E., Hebsgaard, J.B., Nanou, E., Alekseenko, Z., Marklund, U., Kjellander, S., Volakakis, N., et al. (2009). Efficient production of mesencephalic dopamine neurons by Lmx1a expression in embryonic stem cells. Proc. Natl. Acad. Sci. USA *106*, 7613–7618.

Ganat, Y.M., Calder, E.L., Kriks, S., Nelander, J., Tu, E.Y., Jia, F., Battista, D., Harrison, N., Parmar, M., Tomishima, M.J., et al. (2012). Identification of embryonic stem cell-derived midbrain dopaminergic neurons for engraftment. J. Clin. Invest. *122*, 2928–2939.

Grealish, S., Diguet, E., Kirkeby, A., Mattsson, B., Heuer, A., Bramoulle, Y., Van Camp, N., Perrier, A.L., Hantraye, P., Bjorklund, A., et al. (2014). Human ESC-derived dopamine neurons show similar preclinical efficacy and potency to fetal neurons when grafted in a rat model of Parkinson's disease. Cell Stem Cell *15*, 653–665.

Hargus, G., Cooper, O., Deleidi, M., Levy, A., Lee, K., Marlow, E., Yow, A., Soldner, F., Hockemeyer, D., Hallett, P.J., et al. (2010). Differentiated Parkinson patient-derived induced pluripotent stem cells grow in the adult rodent brain and reduce motor asymmetry in Parkinsonian rats. Proc. Natl. Acad. Sci. USA *107*, 15921–15926.

Huang, A.M., Wang, H.L., Tang, Y.P., and Lee, E.H. (1998). Expression of integrin-associated protein gene associated with memory formation in rats. J. Neurosci. *18*, 4305–4313.

Jiang, P., Lagenaur, C.F., and Narayanan, V. (1999). Integrin-associated protein is a ligand for the P84 neural adhesion molecule. J. Biol. Chem. *274*, 559–562.

Joksimovic, M., Yun, B.A., Kittappa, R., Anderegg, A.M., Chang, W.W., Taketo, M.M., McKay, R.D., and Awatramani, R.B. (2009). Wnt antagonism of Shh facilitates midbrain floor plate neurogenesis. Nat. Neurosci. *12*, 125–131.

Kefalopoulou, Z., Politis, M., Piccini, P., Mencacci, N., Bhatia, K., Jahanshahi, M., Widner, H., Rehncrona, S., Brundin, P., Bjorklund, A., et al. (2014). Long-term clinical outcome of fetal cell transplantation for Parkinson disease: two case reports. JAMA Neurol. *71*, 83–87.

Kirkeby, A., Grealish, S., Wolf, D.A., Nelander, J., Wood, J., Lundblad, M., Lindvall, O., and Parmar, M. (2012a). Generation of regionally specified neural progenitors and functional neurons from human embryonic stem cells under defined conditions. Cell Rep. *1*, 703–714.

Kirkeby, A., Nelander, J., and Parmar, M. (2012b). Generating regionalized neuronal cells from pluripotency, a step-by-step protocol. Front. Cell. Neurosci. *6*, 64.

Kirkeby, A., Nolbrant, S., Tiklova, K., Heuer, A., Kee, N., Cardoso, T., Ottosson, D.R., Lelos, M.J., Rifes, P., Dunnett, S.B., et al. (2017). Predictive markers guide differentiation to improve graft outcome in clinical translation of hESC-based therapy for Parkinson's disease. Cell Stem Cell *20*, 135–148.

Kriks, S., Shim, J.W., Piao, J., Ganat, Y.M., Wakeman, D.R., Xie, Z., Carrillo-Reid, L., Auyeung, G., Antonacci, C., Buch, A., et al. (2011). Dopamine neurons derived from human ES cells efficiently engraft in animal models of Parkinson's disease. Nature *480*, 547–551.

La Manno, G., Gyllborg, D., Codeluppi, S., Nishimura, K., Salto, C., Zeisel, A., Borm, L.E., Stott, S.R., Toledo, E.M., Villaescusa, J.C., et al. (2016). Molecular diversity of midbrain development in mouse, human, and stem cells. Cell *167*, 566–580.e19.

Lindvall, O., and Kokaia, Z. (2009). Prospects of stem cell therapy for replacing dopamine neurons in Parkinson's disease. Trends Pharmacol. Sci. *30*, 260–267.

Marei, H.E., Althani, A., Afifi, N., Michetti, F., Pescatori, M., Pallini, R., Casalbore, P., Cenciarelli, C., Schwartz, P., and Ahmed, A.E. (2011). Gene expression profiling of embryonic human neural stem cells and dopaminergic neurons from adult human substantia nigra. PLoS One *6*, e28420.

Metzakopian, E., Lin, W., Salmon-Divon, M., Dvinge, H., Andersson, E., Ericson, J., Perlmann, T., Whitsett, J.A., Bertone, P., and Ang, S.L. (2012). Genome-wide characterization of Foxa2 targets reveals upregulation of floor plate genes and repression of ventrolateral genes in midbrain dopaminergic progenitors. Development *139*, 2625–2634.

Mi, Z.P., Jiang, P., Weng, W.L., Lindberg, F.P., Narayanan, V., and Lagenaur, C.F. (2000). Expression of a synapse-associated membrane protein, P84/SHPS-1, and its ligand, IAP/CD47, in mouse retina. J. Comp. Neurol. *416*, 335–344.

Ohnishi, H., Kaneko, Y., Okazawa, H., Miyashita, M., Sato, R., Hayashi, A., Tada, K., Nagata, S., Takahashi, M., and Matozaki, T. (2005). Differential localization of Src homology 2 domain-containing protein tyrosine phosphatase substrate-1 and CD47 and its molecular mechanisms in cultured hippocampal neurons. J. Neurosci. *25*, 2702–2711.

Ono, Y., Nakatani, T., Sakamoto, Y., Mizuhara, E., Minaki, Y., Kumai, M., Hamaguchi, A., Nishimura, M., Inoue, Y., Hayashi, H., et al. (2007). Differences in neurogenic potential in floor plate cells along an anteroposterior location: midbrain dopaminergic neurons originate from mesencephalic floor plate cells. Development *134*, 3213–3225.

Osafune, K., Caron, L., Borowiak, M., Martinez, R.J., Fitz-Gerald, C.S., Sato, Y., Cowan, C.A., Chien, K.R., and Melton, D.A. (2008). Marked differences in differentiation propensity among human embryonic stem cell lines. Nat. Biotechnol. *26*, 313–315.

Politis, M., Wu, K., Loane, C., Quinn, N.P., Brooks, D.J., Rehncrona, S., Bjorklund, A., Lindvall, O., and Piccini, P. (2010). Serotonergic neurons mediate dyskinesia side effects in Parkinson's patients with neural transplants. Sci. Transl. Med. *2*, 38ra46.

Pruszak, J., Sonntag, K.C., Aung, M.H., Sanchez-Pernaute, R., and Isacson, O. (2007). Markers and methods for cell sorting of human embryonic stem cell-derived neural cell populations. Stem Cells *25*, 2257–2268.

Rath, A., Klein, A., Papazoglou, A., Pruszak, J., Garcia, J., Krause, M., Maciaczyk, J., Dunnett, S.B., and Nikkhah, G. (2013). Survival and functional restoration of human fetal ventral mesencephalon following transplantation in a rat model of Parkinson's disease. Cell Transplant. *22*, 1281–1293.

Reinhold, M.I., Lindberg, F.P., Plas, D., Reynolds, S., Peters, M.G., and Brown, E.J. (1995). In vivo expression of alternatively spliced forms of integrin-associated protein (CD47). J. Cell Sci. *108* (Pt 11), 3419–3425.

Samata, B., Doi, D., Nishimura, K., Kikuchi, T., Watanabe, A., Sakamoto, Y., Kakuta, J., Ono, Y., and Takahashi, J. (2016). Purification of functional human ES and iPSC-derived midbrain dopaminergic progenitors using LRTM1. Nat. Commun. *7*, 13097.

Schumm, M., Lang, P., Bethge, W., Faul, C., Feuchtinger, T., Pfeiffer, M., Vogel, W., Huppert, V., and Handgretinger, R. (2013). Depletion of T-cell receptor alpha/beta and CD19 positive cells from apheresis products with the CliniMACS device. Cytotherapy *15*, 1253–1258.

Shimamura, K., Hartigan, D.J., Martinez, S., Puelles, L., and Rubenstein, J.L. (1995). Longitudinal organization of the anterior neural plate and neural tube. Development *121*, 3923–3933.

Sonntag, K.C., Pruszak, J., Yoshizaki, T., van Arensbergen, J., Sanchez-Pernaute, R., and Isacson, O. (2007). Enhanced yield of neuroepithelial precursors and midbrain-like dopaminergic neurons from human embryonic stem cells using the bone morphogenic protein antagonist noggin. Stem Cells *25*, 411–418.

Steinbeck, J.A., Choi, S.J., Mrejeru, A., Ganat, Y., Deisseroth, K., Sulzer, D., Mosharov, E.V., and Studer, L. (2015). Optogenetics enables functional analysis of human embryonic stem cell-derived grafts in a Parkinson's disease model. Nat. Biotechnol. *33*, 204–209.

Tabar, V., and Studer, L. (2014). Pluripotent stem cells in regenerative medicine: challenges and recent progress. Nat. Rev. Genet. *15*, 82–92.

Verney, C., Zecevic, N., and Puelles, L. (2001). Structure of longitudinal brain zones that provide the origin for the substantia nigra and ventral tegmental area in human embryos, as revealed by cytoarchitecture and tyrosine hydroxylase, calretinin, calbindin, and GABA immunoreactions. J. Comp. Neurol. *429*, 22–44.

Villaescusa, J.C., and Arenas, E. (2010). Transplantable midbrain dopamine neurons: a moving target. Exp. Neurol. *222*, 173–178.

Wood, H.B., and Episkopou, V. (1999). Comparative expression of the mouse Sox1, Sox2 and Sox3 genes from pre-gastrulation to early somite stages. Mech. Dev. *86*, 197–201.